UNIVERSITY OF PARDUBICE
FACULTY OF TRANSPORT ENGINEERING

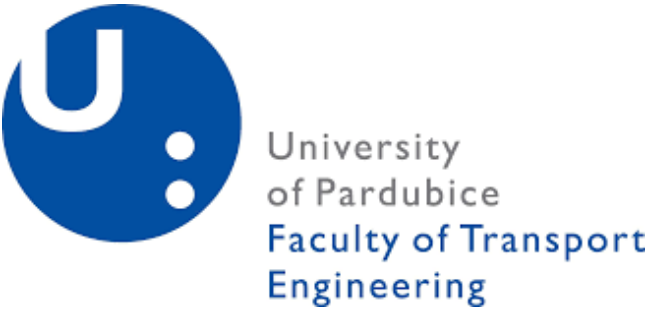

PROBABILISTIC NONLINEAR COMPUTER SIMULATIONS FOR REALISTIC PREDICTION OF STRUCTURAL RESPONSE

ÖZGÜR YURDAKUL

A THESIS SUBMITTED FOR
THE DEGREE OF DOCTOR OF PHILOSOPHY

2019

Program of Study:
P3710 - Technique and Technology in Transport and Communications

Branch of study:
3706V005 - Transport Means and Infrastructure

Dissertation Title:
Probabilistic Nonlinear Computer Simulations for Realistic Prediction of Structural Response

Author:
Özgür YURDAKUL

Supervisor:
Ing. Ladislav ŘOUTIL, Ph.D.

The dissertation has arisen at the supervising:
Faculty of Transport Engineering, Department of Transport Structures

ABSTRACT

Özgür YURDAKUL

University of Pardubice
Department of Transport Structures

The effect of inherent uncertainties in material properties on the global response of substandard reinforced concrete (RC) structural members was investigated by the stochastic study. An experimentally validated finite element model (FEM) was, therefore, combined with a suitable stochastic sampling technique (Latin Hypercube Sampling (LHS)). Then, the effect of inherent uncertainties on the material mechanical properties was studied by uncertainty analysis, while the uneven distribution of concrete mechanical properties over the specimen was accurately characterized by random fields theory. The partial correlation coefficient between material parameters and response variables was also evaluated to outline the parameters which mainly contribute to the global response (i.e., sensitivity analysis). Such an advanced modelling strategy was implemented on three different testing programs comprising RC members designed with structural details and material properties non-conforming to current codes and guidelines. The first testing program deals with experimental performance of an over-reinforced and shear critical beams together with stochastic assessments of beam members via computational stochastic mechanics. The effect of uncertainties on the response of shear critical and carbon fiber reinforced polymer (CFRP) retrofitted beam-column joints, which were selected from available testing programs in the literature, was also discussed. The stochastic-based numerical prediction of beam-type RILEM bond specimens characterized variability in the identical tests satisfactorily. Owing to the more realistic assessment capability of the stochastic-based nonlinear finite element (FE) analysis, the global response of the substandard RC members (over-reinforced and shear critical beams; shear critical and CFRP retrofitted beam-column joints; beam-type RILEM bond specimens) was accurately reproduced.

Keywords: Reinforced Concrete, Substandard, Sensitivity; Stochastic Assessment; Finite Element Method, Nonlinear Analysis, Uncertainty, Random Fields

1 INTRODUCTION

According to the capacity design principles specified in most modern codes and guidelines, structural members should exhibit a ductile response. The requirements to meet the ductile behavior and design principles are carefully described in the relevant documents. However, a significant portion of RC buildings in the existing building inventory of both developed and developing countries have specific deficiencies at the local level, which usually cause premature failure of structural members. Severe damage at the member remarkably violates the integrity of the structural system. The obvious outcomes are poor energy dissipation and sudden degradation of strength and stiffness. As local damages also actuate the global failure mechanism, investigating the behavior of substandard members is essential. Based on field observations and laboratory tests, capacity design principles have earmarked deficient RC members as critical components in the moment-resisting frames. It is, therefore, important to pay enough attention to the assessment of RC members with local deficiencies.

Several attempts have been made to investigate the response of substandard RC members by using experimental and numerical methods. However, further developments are urgently needed due to the randomness in either material properties or strength distribution over specimen geometry. Therefore, a more advanced method, which combines the nonlinear FEM with the stochastic sampling technique, is required. Owing to the more realistic assessment capability of the stochastic-based nonlinear FE analysis, which is available in user-friendly computer tools, reproducing the structural response of substandard members using computational stochastic mechanics could yield more accurate results for assessment purposes. Therefore, a focus on the probabilistic nonlinear computer simulations should be given.

In this study, different kinds of failure modes in substandard RC members were assessed by using stochastic approaches. For this reason, the nonlinear FEM was combined with a suitable stochastic sampling technique for the realistic prediction of the structural response in substandard RC members. Overall, the effect of inherent uncertainties on the material mechanical properties was studied by using uncertainty analysis, which leads to obtaining the basic statistics of response variables. The sensitivity of material properties

on the global response was also measured by evaluating the partial correlation coefficient between material parameters (i.e., input variables) and strength parameters (i.e., response variables). Moreover, the uneven distribution of concrete mechanical properties over the specimen was accurately characterized by random fields theory, which establishes weaker and stronger spots over the specimen. All of these provided a broad perspective in assessing the results.

The stochastic approach was implemented in three different testing programs. The first testing program deals with over-reinforced and shear critical beams. The experimental performance of two substandard beam specimens was first obtained and then accurately reproduced in the FE environment. The effect of inherent uncertainties at a material level for an over-reinforced and shear critical beam, and the uneven distribution of concrete mechanical properties over the shear critical beam were handled by an uncertainty analysis and random fields approach, respectively. The stochastic assessment of shear critical and CFRP retrofitted beam-column joints, which were selected from available testing programs in the literature, was also investigated. The experimental performance of shear failed joints, and CFRP fracture was closely estimated by using the stochastic approach. The relative impact of each material properties on the shear critical and CFRP retrofitted joints was then provided, which remarks the most critical material parameters affecting the global response. The third testing program focused on the stochastic-based numerical prediction of beam-type RILEM bond specimens. The proposed bond stress-slip relations, which were evaluated from the experimental data, were first implemented in the FE models. Thus, the deterministic numerical models accurately reproduced the experimental performance of confined and unconfined specimens under cyclic and monotonic loading. The variability in the identical tests was satisfactorily characterized by the stochastic assessment.

To conclude, the stochastic approach described in this study was implemented on three different testing programs. The performance of the advanced assessment method on different failure modes, which combines the nonlinear finite element method with the stochastic sampling technique, was evaluated.

2 MODELLING PARAMETERS

As the computer-aided nonlinear analysis is now available for RC members, refined numerical models allow for reproducing the response of substandard members with satisfactory accuracy. This chapter briefly presents the numerical modeling strategies in a user-friendly computer tool ATENA software [1], used for different RC members that have exhibited different failure types.

The concrete geometry was modeled using the hexahedral element *CCIsoBrick*. The constitutive models of tensile and compressive behaviors were combined in *CC3DNonLinCementitious2* (a fracture-plastic concrete model) in the software. Moreover, the *Reinforced Concrete* material model provides an opportunity to model the reinforcement in a smeared manner. An elliptical hardening and linear softening behavior were assumed in defining the uniaxial compressive behavior of the concrete [2]. Accordingly, a strain-based hardening response was followed by a displacement-based linear softening response in compressive. The relation in the form of the Gaussian curve was implemented to reduce the compressive strength in cracked concrete while its parameters were obtained from available literature [3,4]. Menetrey and Willam criteria [5] was implemented for the definition of the failure surface in the numerical model. The behavior of plain concrete under tension was assumed to be uncracked in the elastic region while an exponential softening response between the stress in the crack σ and crack width w was adopted in the post-elastic region [6]. The crack width at complete stress release w_c was evaluated by the relation between fracture energy G_f and displacement w [6]. The smeared crack concept in combination with crack band theory [7] was implemented in the software for the strain-displacement relation. The stress in the crack is not completely released in the heavily reinforced members due to the strength provided by the reinforcing bar. Therefore, tensile softening behavior was modified accordingly in the beam and column by using the relation proposed in CEB-FIP Model Code [8].

The longitudinal reinforcing bars were defined as truss elements with a bilinear elastoplastic model, considering the hardening behavior. It was modeled as a discrete reinforcement embedded in the concrete geometry. Menegotto and Pinto [9] model for the nonlinear cyclic material behavior of the

reinforcing steel was employed. The reinforcing bar was fully connected to the surrounding concrete geometry with the limited bond strength, which is defined by a *CCBarWithBond* type element [1].

The CFPR sheets were modeled using membrane elements with composite material properties. Namely, the CFRP net was defined by the smeared reinforcement concept by the *Reinforced Concrete* material model, which combines the brittle material with reinforcement [10]. Therefore, the brittle response of epoxy resin was defined as that of a fracture/plastic material (i.e., *CC3DNonLinCementitious2*), while the CFRP was modeled as a smeared reinforcement. The bond between the concrete surface and CFRP sheet was characterized by inserting a supplementary surface (an interface) between the two materials. The interface material is based on Mohr-Coulomb criterion [11].

The efficiency of the numerical model is strongly related to the mesh size as it has vital importance on the accuracy of numerical results. The mesh size was optimized by trying different mesh size until the variation in the computed maximum load is minimized.

3 STOCHASTIC STUDY

3.1 Uncertainty Analysis

The randomness in the material properties can be simulated by computational stochastic fracture mechanics. Hence, the deterministic model was evolved to the stochastic level. Sets of input parameters were simulated by a stratified sampling technique (i.e., Latin Hypercube Sampling (LHS)) using defined distribution functions. The deterministic values with their distribution, and the correlation among the material parameters are presented in Table 1, and Table 2, respectively. Those are based on experimental observations, Pukl *et al.* [12], fib Bulletin No.22 [13], Gulbrandsen [14], Atadero and Karbhari [15], Baji *et al.* [16] and Joint Committee on Structural Safety (JCSS) [17].

A set of load-displacement curves was achieved as the outcome of the performed analyses with generated samples. The distribution of the ultimate load (i.e., response variable) corresponding to each cycle was obtained from that bundle. Moreover, basic statistics of the response variable (e.g., mean value, standard deviation, and PDFs of capacity) were provided. Finally, the

Spearman rank-order correlation coefficient between the generated input and response variables was found. The major material parameters characterizing the overall behavior of the specimens were thus provided.

Table 1. Material properties as random parameters and their statistical distributions

Parameter	Mean Value, μ	COV	Distribution
	Concrete		
Elastic Modulus, E_c (MPa)	$4700\sqrt{f_c}$ [18]	0.10	Lognormal (2 Parameter)
Tensile strength, f_{ct} (MPa)	$0.30f_c^{2/3}$ [8]	0.30	Lognormal (2 Parameter)
Compressive Strength, f_c (MPa)	8.05 EJ-R 9.40 EJ-C	0.15	Lognormal (2 Parameter)
Fracture Energy, G_f (N/m)	$73f_{ct}^{0.18}$ [8]	0.25	Weibull (2 Parameter)
Compressive Strain, ε_{co} (mm/mm)	f_c/E_c [2]	0.15	Lognormal (2 Parameter)
Plastic Displacement, w_d (m)	Linear [19]	0.10	Lognormal (2 Parameter)
	Reinforcing Steel		
Elastic Modulus, E_s (GPa)	190.9	0.07	Lognormal (2 Parameter)
Yield Strength, f_y (MPa)	295.5	0.07	Lognormal (2 Parameter)
Ultimate Strength, f_u (MPa)	437.5	0.07	Lognormal (2 Parameter)
Ultimate Strain, ε_u (mm/mm)	0.21	0.07	Normal
	CFRP		
Elastic Modulus, E_f (GPa)	230	0.08	Lognormal (2 Parameter)
Tensile Strength, f_f (MPa)	4900	0.08	Lognormal (2 Parameter)
Effective thickness, t_f (mm)	0.111	-	Deterministic
	MBT-MBrace® Adesivo (Saturant)		
Elastic Modulus, E_{as} (MPa)	1800	0.10	Lognormal (2 Parameter)
Compressive Strength, f_{cas} (MPa)	80	0.15	Lognormal (2 Parameter)
Tensile strength, f_{ctas} (MPa)	12	0.30	Lognormal (2 Parameter)
Fracture Energy, G_{fas} (N/m)	100 [20]	0.25	Weibull (2 Parameter)
Compressive Strain, ε_{cos} (mm/mm)	f_{cas}/E_{as} [2]	0.15	Lognormal (2 Parameter)
Plastic Displacement, w_d (m)	Linear [2]	0.10	Lognormal (2 Parameter)

Table 2. Correlation coefficients among the random parameters

Concrete and Adesivo (Saturant)					
	E_c	f_c	f_{ct}	G_f	ε_{co}
E_c	1	0.70	0.60	0.40	0.90
f_c		1	0.70	0.50	0.90
f_{ct}			1	0.80	0.60
G_f		SYM		1	0.50
ε_{co}					1

Steel				
	E_s	f_y	f_u	ε_u
E_s	1	0	0	0
f_y		1	0.75	0.45
f_u	SYM		1	0.60
ε_u				1

CFRP		
	E_f	f_f
E_f	1	0.31
f_f	SYM	1

3.2 Random Fields Theory

The response of the structural member is influenced by the uneven distribution of the concrete mechanical properties. For this purpose, the uncertainties in the distribution of the concrete mechanical properties over the specimen were described as random variables. This randomness was considered via the random fields approach [21]. The samples from the statistical analyses were the input parameters (listed in Table 1) for the nonlinear FE solutions. In the refined numerical models, these input parameters were not distributed evenly, but were established as weaker and stronger regions over the specimen. In other words, the concrete mechanical properties changed with the geometric coordinates, causing variability over the specimen. The random fields for each prominent material parameter were generated in FReET [22]. The deterministic model was then modified in SARA Studio [23], which interfaces the statistical analysis (i.e., FReET results) to FE software, enabling probabilistic nonlinear analyses.

4 CASE I: BEAM TEST

Two different failure modes of RC beam members, which include concrete crushing due to reaching the limit strain of the concrete in compression and excessive shear failure, were examined using experimental and stochastic methods.

4.1 Experimental Program

A series of tests on the shear critical and over-reinforced beams were conducted in cooperation with Structural Mechanics Laboratory, Department of Civil Engineering, Eskişehir Technical University, Turkey. The experimental program consists of a four-point bending test on the shear deficient and over-reinforced substandard RC beam specimens. While the shear critical beam was designed without any transverse reinforcement to achieve excessive shear failure by exceeding the tensile strength of the concrete, the over-reinforced beam was designed with reinforcement detailing, resulting in concrete crushing. The specimens were constructed from low strength concrete. The details of the specimens are depicted in Fig. 4.1a and b, respectively.

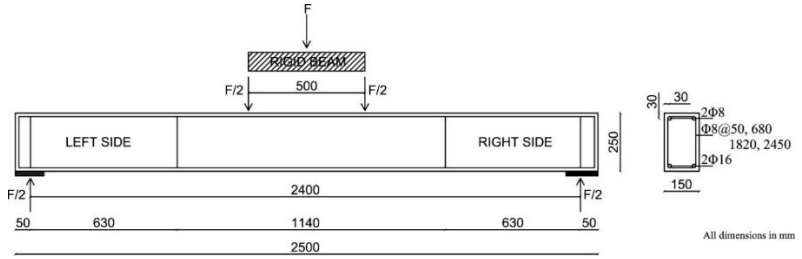

(a)

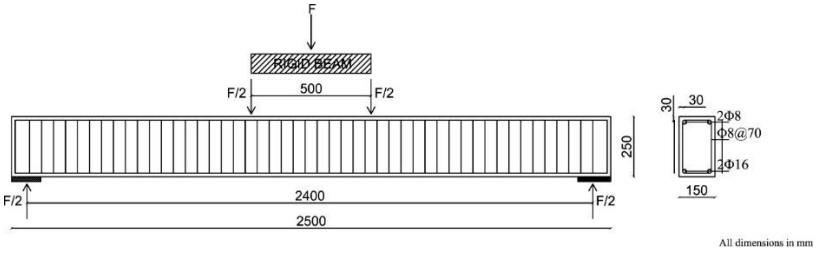

(b)

Fig. 4.1. Reinforcement scheme and dimension details (a) shear critical specimen, EB_R (b) over-reinforced specimen, EB_C

The summary of the test specimens is presented in Table 4.1.

Table 4.1. Description of test specimens

	Specimen	
	EB_R	EJ_C
Description	Shear Critical	Over-Reinforced
Reinforcement Scheme	Fig. 4.1a	Fig. 4.1b
Concrete Compressive Strength, f_c (MPa)	15.0	17.1
Elastic Modulus, E_s (GPa)	200	
Yield Strength, f_y (MPa)	460	
Ultimate Strength f_u (MPa)	632	
Ultimate Strain, ε_u (mm/mm)	0.17	
Beam Dimension	150 x 250 x 2500 mm	
Longitudinal Reinforcement	2ϕ16+2ϕ8	4ϕ16+2ϕ8
Transverse Reinforcement	ϕ8@50, 680 1820 and 2450 mm	ϕ8/70
Application of Displacement	Four-Point Bending	
Loading Protocol	Monotonic	
Failure Mode	Shear Failure	Concrete Crushing

4.2 Over-Reinforced Beam

The exhibited performance of the specimen was a brittle type of failure as a result of concrete crushing caused by reaching the limit strain of the concrete in compression (Fig. 4.2a). The stress distribution along the specimen's longitudinal axis and crack pattern are depicted in Fig. 4.2b. The resulting failure mode was predicted well by the numerical assessment. Concrete crushing in the compression zone was in good agreement with the compressive stress distribution obtained from FE analysis. The flexural hairline cracks in the tension zone were also captured by the numerical solution.

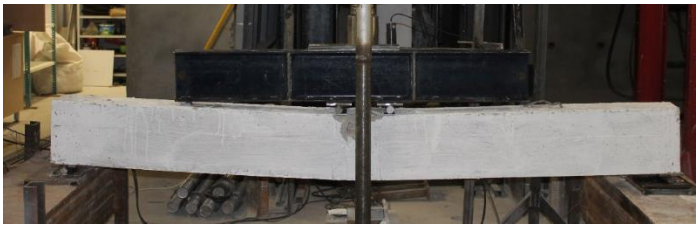

(a)

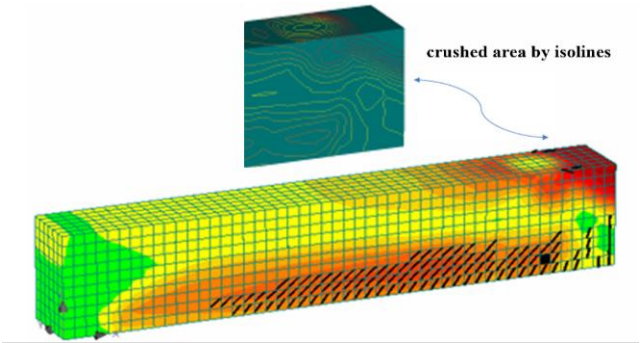

(b)

Fig. 4.2. (a) Concrete crushing in the over-reinforced beam (b) numerical prediction at failure

The deterministic FE model, which was modeled with the average values of the material parameters, matched well with the experimental capacity with an error of 10%. The set of load-displacement curves formed a band around the deterministic model, which was also covered by the experimental results (Fig. 4.3). The stochastic bundle also provided the upper and lower boundaries of the

load, corresponding to each displacement level. The scatter was higher in the subsequent displacement due to the effect of different nonlinear mechanisms.

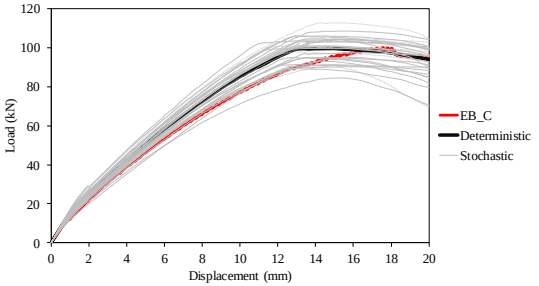

Fig. 4.3. Set of load-displacement curves in over-reinforced beam

4.2.1 Reliability Analysis of Over-Reinforced Beam

The PDF of the load, which corresponds to the critical deflection *L/250* described in EN 1992-1-1 [24], was obtained from the stochastic bundle. After that, the safety margin was obtained by subtracting capacity (i.e., resistance) from demand (i.e., load). Finally, the load corresponding failure probability, related to the irreversible serviceability limit state, was computed as 73.5 kN (Fig. 4.4a). Namely, the values smaller than 73.5 kN are safe according to the reliability concept. The PDF of the ultimate loads is found as well for the over-reinforced beam (Fig. 4.4b). The load corresponding failure probability, related to the irreversible serviceability limit state, was computed as 79.2 kN.

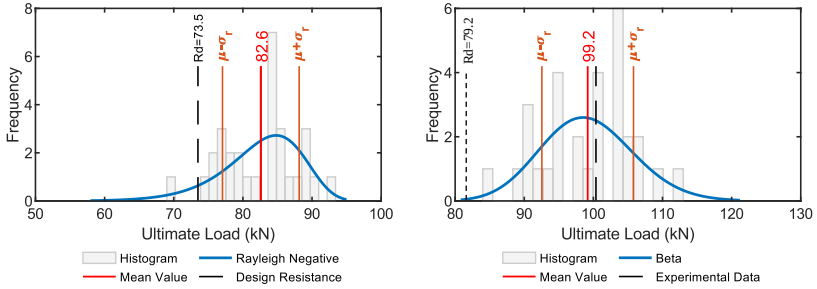

Fig. 4.4. PDF of (a) serviceability limit state (b) ultimate limit state

4.2.1 Sensitivity Analysis of Over-Reinforced Beam

The relative impact of concrete compressive strength f_c was the most considerable among others as it has the highest correlation (Fig. 4.5). Thus, the experimental and numerical responses, which were characterized by concrete crushing due to reaching the limit strain of concrete, were also ascertained by the sensitivity analysis. The tensile strength of concrete f_{ct} influenced the global response remarkably. It is worthy to mention that flexural cracks also appeared during the test. Thus, the tensile strength of concrete f_{ct} became critical up to a certain level of displacement. The sensitivity measures on the remaining materials showed a low correlation coefficient. Thus, their relative impact on the global response was not significant.

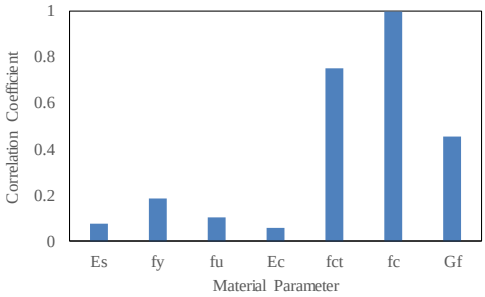

Fig. 4.5. Sensitivity of material properties in EB_C

4.3 Shear Critical Beam

The spatial variability of the concrete mechanical properties along the specimen vitally affects the capacity, initial stiffness, and ultimate displacement of the specimen. These behaviors were clearly identified in the presented stochastic bundle of load–displacement curves. The randomized concrete strength did not influence the linear response of the specimen, but remarkably affected the nonlinear response of the concrete. The shear failure caused severe damage on the left side of the beam (Fig. 4.6a). On the other hand, the crack pattern in the deterministic FE analysis was distributed almost evenly on both sides of the specimen (Fig. 4.6b). The random fields theory accounts for variability in the concrete mechanical properties. The possible crack patterns in some of the selected analyses are presented in Fig. 4.6c. As depicted in the

figures, the crack pattern obtained in each analysis considerably depended on the randomness.

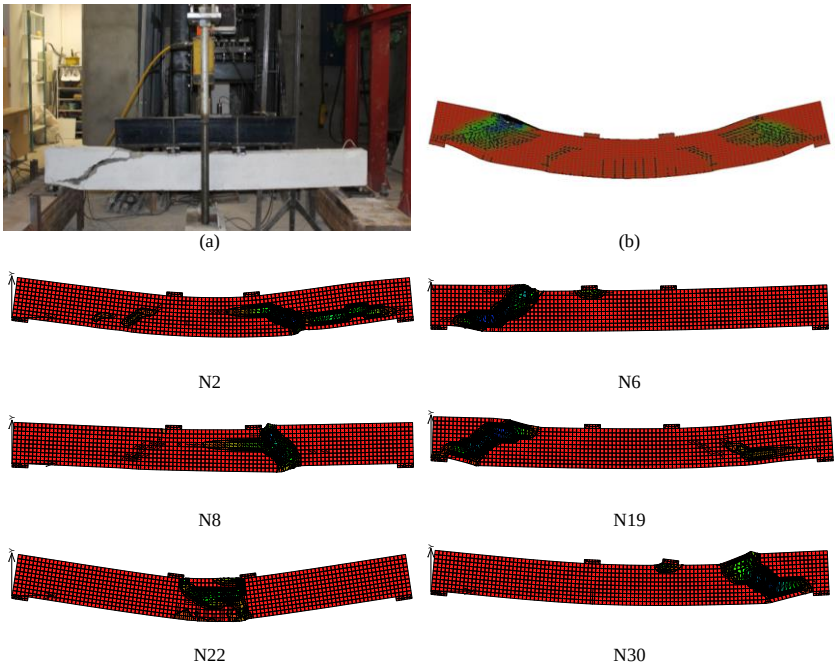

Fig. 4.6. Damage state at failure: (a) experiment (b) deterministic model (c) random fields

Fig. 4.7 shows the range of load-displacement curves for beams with different material properties. The stochastic approach provided the possible ranges of load-displacement curves. As the geometrical position of the weakest spot defines the failure mode and capacity, the load-displacement curves in the stochastic analysis did not form a band around the deterministic model. The important point in such predictions is that the experimental results to be used for the assessment of the member (i.e., the observed initial stiffness, peak load, failure mode, and crack pattern) could be covered by the stochastic model.

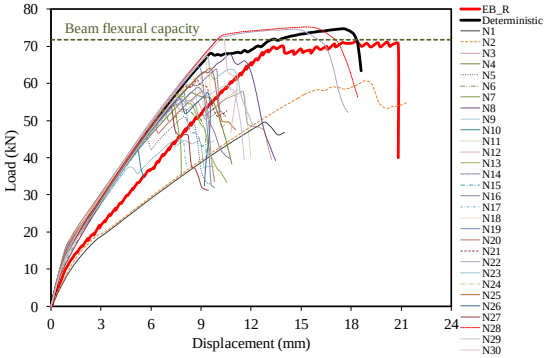

Fig. 4.7 Set of load-displacement curves

5 CASE II: JOINT TEST

The effect of inherent uncertainties in material constitutive models on the response of substandard as-built and CFRP retrofitted RC beam-column joints was investigated through a stochastic study.

5.1 Selected Experimental Tests

The experimental tests used to validate the proposed numerical models collected from two different testing programs previously conducted by the author: Yurdakul [25], Yurdakul and Avşar [26,27], and Yurdakul *et al.* [28]. The full-scale test specimens, which represent the exterior beam-column joint, were constructed by considering the most common deficiencies. Geometrical parameters and material properties were selected in such a way that they would characterize the construction practices of the existing deficient beam-column subassemblies (Fig. 5.1a and b).

5.1.1 Structural Retrofit

The design philosophy in the rehabilitation of specimens is to attain the initial capacity, upgrading the performance of structural members, delaying or eliminating brittle failure modes, and initiating the formation of flexural plastic hinges in the beam to attain a ductile behavior [29]. In dimensioning CFRP sheets, it was assumed that the lateral load causing beam yielding without joint failure will be carried only by the corresponding CFRP sheets (Fig. 5.1c).

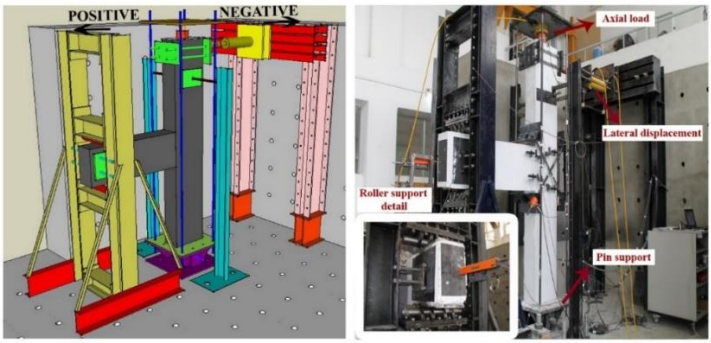

(a)

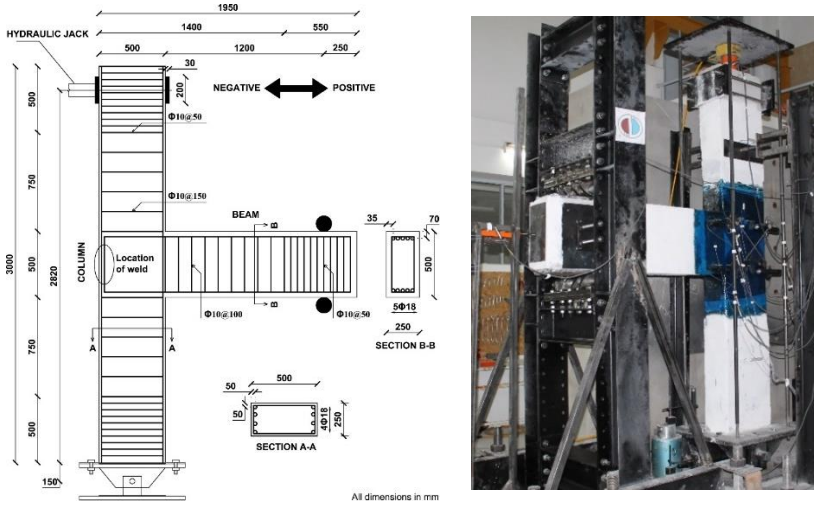

(b) (c)

Fig. 5.1. a) 3D view of the selected specimen (b) dimension and reinforcement details of the subassembly (c) CFRP retrofitted specimen [25,27]

5.2 Hysteric Response

The overall response of the reference specimen representing the as-built subassembly (EJ-R) was dominated by the joint shear failure, which results in premature failure of the RC member. When the deterministic model evolved to the stochastic level, the scatter with the possible range of the load for each drift level can be seen in Fig. 5.2a and b.

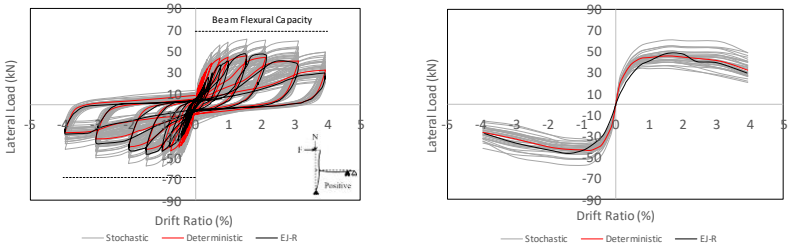

(a) (b)

Fig. 5.2. (a) Hysteric response of reference specimen, EJ-R (b) envelope curve of hysteresis loops

The resulting large corner-to-corner cracks in the joint panel and propagated cracks at the joint back were reasonably reproduced by the deterministic numerical assessment of the reference specimen (Fig. 5.3a-c). As the imposed displacement increases, new hairline cracks spread over the whole beam (Fig. 5.3a and b). In the subsequent drift levels, the existing cracks in the joint panel widened while those propagated in the beam almost closed (Fig. 5.3b and c).

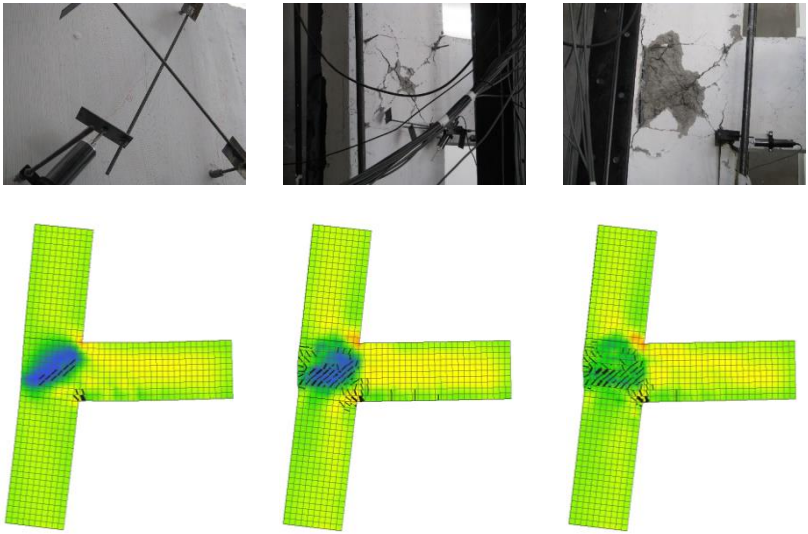

0.2% Drift Ratio (First crack) 2% Drift Ratio 4% Drift Ratio (Failure)

(a) (b) (c)

Fig. 5.3. Comparison of crack pattern obtained by experimental response and deterministic numerical model for the reference specimen (EJ-R) (a) first joint cracking (b) 2% drift ratio (c) 4% drift ratio

The specimen incorporating the retrofit solution via CFRP wrapped in an X pattern (EJ-C) suffered from diagonal cracks after a certain level of displacement corresponding to CFRP debonding/rupture. Therefore, the specimen displayed a non-ductile behavior together with the distinct strength deterioration and stiffness degradation due to the shear failure of the joint after CFRP rupture. A set of load-displacement curves along with both the experimental response and numerical assessment is depicted in Fig. 5.4a and b for the retrofitted specimen.

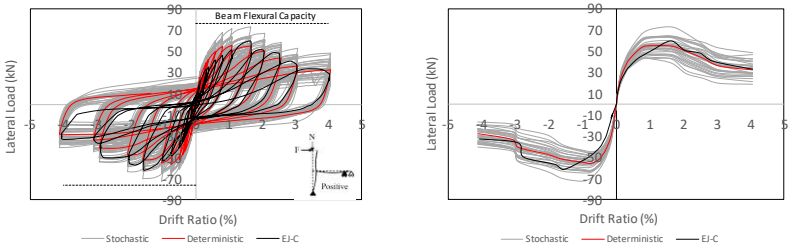

(a) (b)

Fig. 5.4. (a) Hysteric response of retrofitted joint, EJ-C (b) envelope curve of hysteresis loops

The deterministic numerical assessment well captured the crack pattern together with the resulting failure mode. The severe joint shear cracks at failure were also monitored in the deterministic model. Moreover, the vertical splitting cracks at the beam-joint interface were closed partially in the beam, which was accurately reproduced in the FE model as well (Fig. 5.5a-c).

5.2.1 Analysis of Results

The ultimate strength of the specimen is one of the important parameters in the cyclic response assessment of specimens. Basic statistical parameters related to the ultimate strength were, therefore, provided in Fig. 5.6a and b. The PDFs of peak strength and their statistical parameters (i.e., mean value and standard deviation) were obtained from the series of data points (i.e., ultimate capacity of each analysis). For the fitted distributions, Chi–square or Kolmogorov–Smirnov tests, which measure the goodness of the fit, are satisfied at the 95% confidence level. Then, the mean value of predicted peak strength was compared with the experimentally obtained capacity.

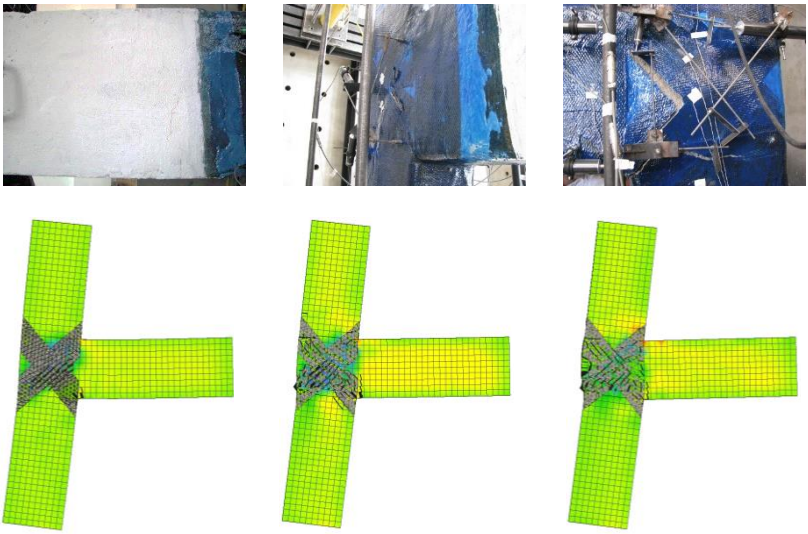

0.2% Drift Ratio (First beam crack) 2% Drift Ratio 4% Drift Ratio (Failure)

(a) (b) (c)

Fig. 5.5. Comparison of crack pattern obtained by experimental response and deterministic numerical model for the retrofitted specimen (EJ-C) (a) first joint cracking (b) 2% drift ratio (c) 4% drift ratio

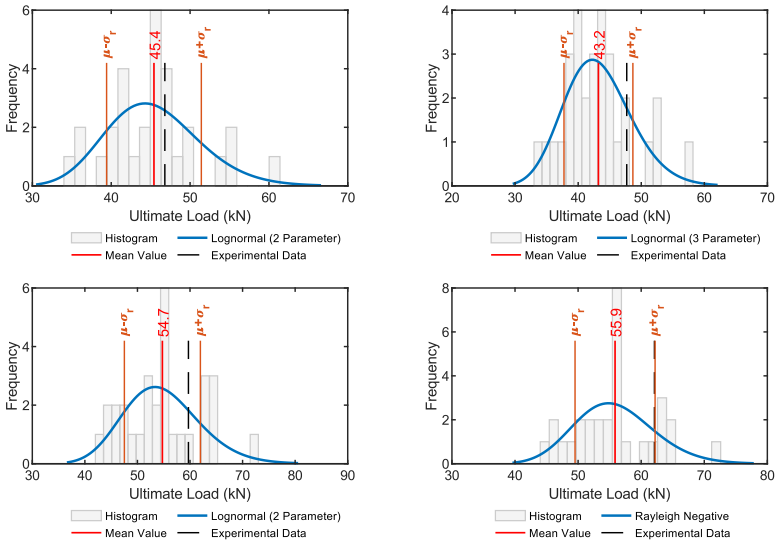

Positive Loading Direction Negative Loading Direction

Fig. 5.6. (a) PDFs of EJ-R (b) PDFs of EJ-C

5.3 Sensitivity Analysis

The contribution of the concrete tensile strength f_{ct} to the global response was the most significant, because it had the highest correlation coefficient for the positive and negative loading direction of the reference specimen. (Fig. 5.7a and b). The relative impact of the concrete compressive strength f_c on the global response was also considerable. This phenomenon can be attributed to the development of the diagonal compression strut mechanism, which is perpendicular to the tension tie at the joint panel. The remaining material properties had a weak influence on the global response as the correlation coefficients are rather low (in some cases very close to zero).

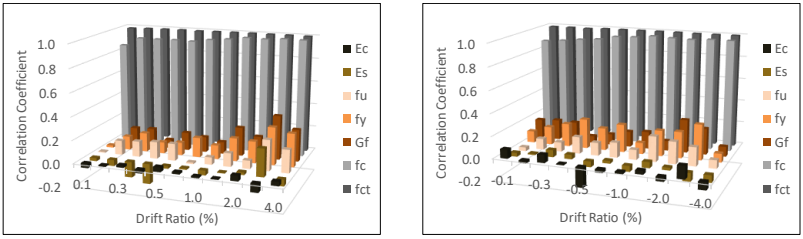

(a) (b)

Fig. 5.7. Sensitivity analysis in the reference specimen EJ-R (a) positive loading direction (b) negative loading direction

The sensitivity measures resulted in high correlation with three input variables of the retrofitted specimens, which included the tensile strength of concrete f_{ct}, compressive strength of concrete f_c, and tensile strength of epoxy resin f_{ctas} (Fig. 5.8a and b). A gradual increment was observed in the correlation coefficient of the concrete compressive strength f_c.

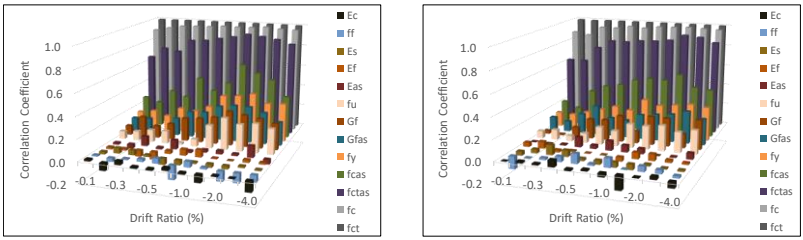

(a) (b)

Fig. 5.8. Sensitivity analysis in the retrofitted specimen (a) positive loading direction (b) negative loading direction

6 CASE III: BOND TEST

This chapter deals with the exhibited performance of beam-type RILEM bond specimens and their stochastic assessment by computational stochastic mechanics.

6.1 Experimental Program

The principle of the test described in this section is based on RILEM recommendation [30] and EN 10080 [31]. A beam specimen is tested under flexure by a four-point bending test (Fig. 6.1a). The failure criterion is the complete loss of adhesion in one half of the beam or failure of reinforcing steel. The axial stress in the reinforcing bar is transmitted to the surrounding concrete surface through shear stress.

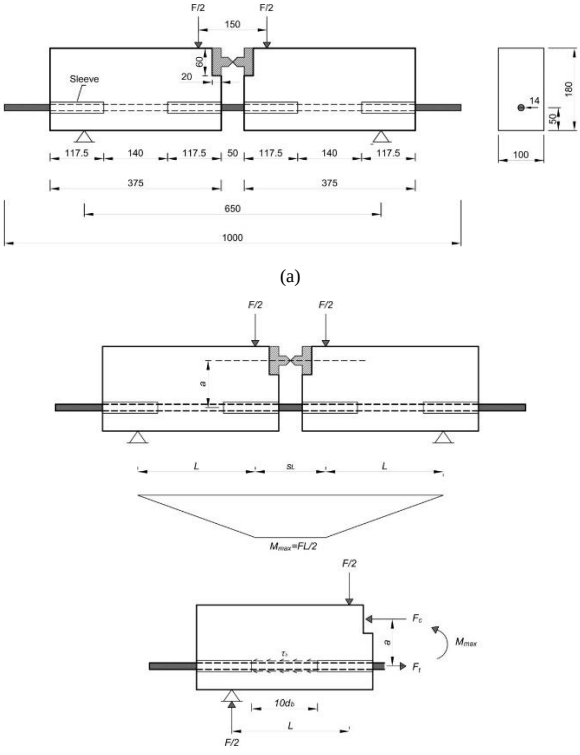

Fig. 6.1. (a) Beam test specimen detail for d_b=14 mm (b) load transfer mechanism [31]

The experimental program consists of two testing groups (Fig. 6.2). The test samples in both groups were identical in terms of material properties and dimensions but differ in testing methodology. The first test group was exposed to the monotonic loading, while the second one was tested under reverse cyclic loading. Each group was then divided into two testing series. The first test series was constructed without transverse reinforcement. The bond behavior in plain concrete was, therefore, investigated. The second series contains test specimens with transverse reinforcement so that the effect of confinement provided by the shear reinforcement can be revealed.

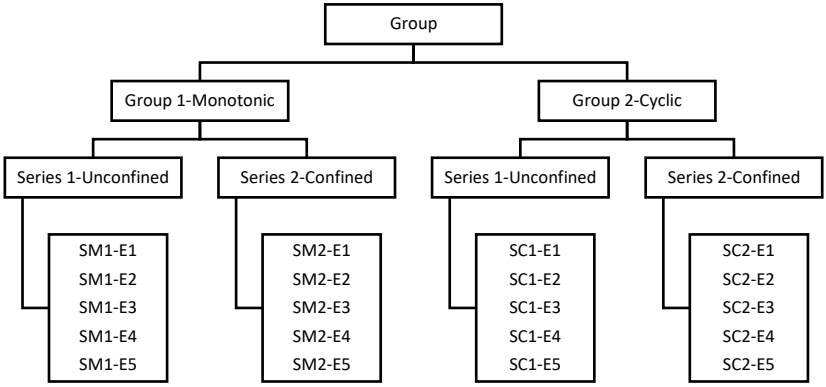

Fig. 6.2. Summary of test specimens

6.1.1 Monotonic Test Setup

The four-point bending test setup with a symmetrical configuration was designed. The specimens were tested under monotonic loading up to failure. The specimens were placed horizontally and then loaded vertically. The displacement was applied at mid-span by a hydraulic jack acting vertically through rigid steel plates. The hydraulic jack was placed to an adjustable steel frame that allows movement in both horizontal and vertical directions. The top-end of the actuator was fixed to the steel frame by a steel plate while a cardan joint was attached to the jack from the bottom-end (Fig. 6.3).

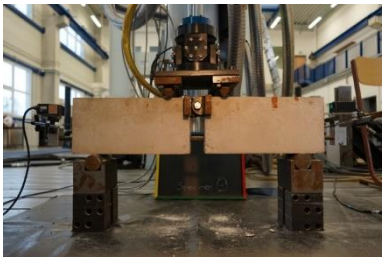

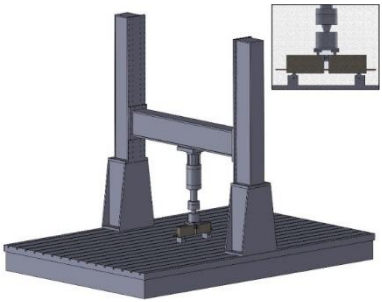

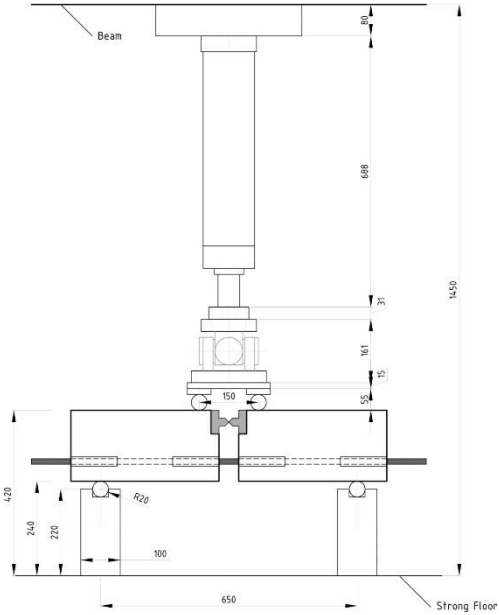

Fig. 6.3. Detail of monotonic test setup

6.1.2 Cyclic Test Setup

The ordinary arrangement of the supports in the monotonic test setup is a pin and roller configuration on each side of the specimen. The loading is provided by two loading rollers placed at an equal distance around the middle of the beam. Then, the specimen sitting on the supports is imposed to load lowered from the above without clamping. This does not bring any indeterminacy in a bent beam since the axial deformations are not restricted.

On the other hand, such a test setup configuration results in an instability under reverse cyclic loading since it is not supported during unloading. Thus, the test setup in monotonic cyclic loading is not capable of performing tests under reverse cyclic loading. Therefore, the monotonic four-point bending test setup must be modified for the cyclic tests. Soleymani *et al.* [32] adapted a suitable support-clamping mechanism, which allows one to load and support the specimen under reverse cyclic loading in a stable manner (Fig. 6.4).

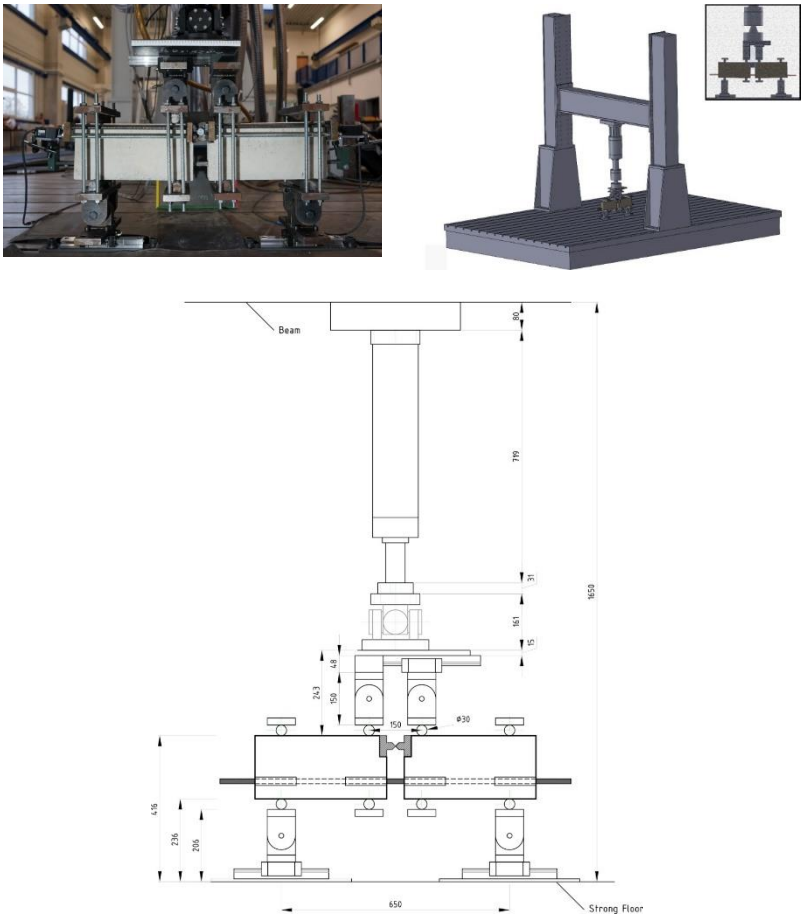

Fig. 6.4. Detail of cyclic test setup

6.2 Bond-Slip Relation for Monotonic Loading

6.2.1 Proposed Bond Model for Unconfined Concrete

Five identical specimens were tested under the same conditions and then the bond strength for each specimen was evaluated. The bond stress was computed as the ratio between axial force in the reinforcing bar and surface area. The analytical relationship (see equations below) was proposed by fitting a curve (i.e., the method of least squares) to the mean experimental data (Fig. 6.5).

$$\tau_u(s) = \begin{cases} \tau_{u1}\left(\frac{s}{s_{u1}}\right)^{\alpha} & if\ s < s_{u1} \\ 0.015s^2 - 0.15s + 0.71 & if\ s_{u1} \le s \le s_{u2} \\ \tau_{u2} & otherwise \end{cases} \quad \text{Eq. 6.1}$$

where the variables in the formula defined as follows:

$$\tau_{u1} = 0.63 f_c^{\,1/4} \quad \text{Eq. 6.2}$$

$$\tau_{u2} = 0.53 \times \tau_{u1} \quad \text{Eq. 6.3}$$

$$\alpha = 0.15 \quad \text{Eq. 6.4}$$

$$s_{u1} = \sqrt{\frac{f_c}{40}} \quad s_{u2} = 5.0 \quad \text{Eq. 6.5}$$

Here, τ_{u1} and τ_{u2} are the maximum and residual bond strength values. s_{u1} and s_{u2} are the slip values at the ultimate and residual bond strength, respectively. α is a shape factor.

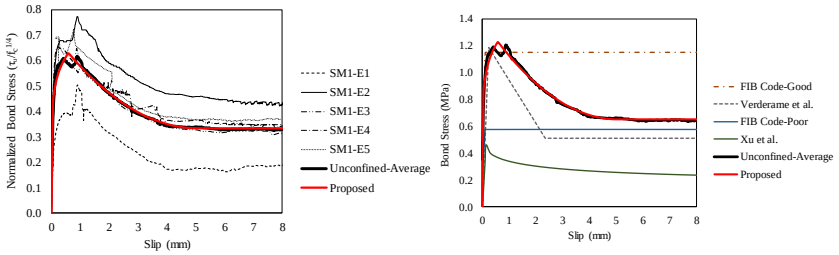

(a) (b)

Fig. 6.5. (a) Proposed bond-slip model for unconfined concrete under monotonic loading (b) comparison with available models

6.2.2 Proposed Bond Model for Confined Concrete

The three-segment curve, which was evaluated by data analysis (i.e., curve fitting to an average of experimental data), was also proposed for the confined concrete (Fig. 6.6).

$$\tau_c(s) = \begin{cases} \beta_c \times \left[\tau_{c1} \left(\frac{s}{s_{c1}} \right)^{\alpha} \right] & if\ s < s_{c1} \\ \beta_c \times [0.01s^2 - 0.11s + 0.782] & if\ s_{c1} \le s \le s_{c2} \\ \beta_c \times \tau_{c2} & otherwise \end{cases} \quad \text{Eq. 6.6}$$

where the variables in the formula defined as follows:

$$\tau_{c1} = 0.69 f_c^{1/4} \quad \text{Eq. 6.7}$$

$$\tau_{c2} = 0.70 \times \tau_{c1} \quad \text{Eq. 6.8}$$

$$\alpha = 0.20 \quad \text{Eq. 6.9}$$

$$s_{c1} = \sqrt{\frac{f_c}{12}} \quad s_{c2} = 6.0 \quad \text{Eq. 6.10}$$

$$\beta_c = 0.855 e^{f_e / \frac{2}{f_c^3}} \text{ for } f_e \ge 0.05 \quad \text{Eq. 6.11}$$

Here, τ_{c1} and τ_{c2} are the maximum and residual bond strength values. s_{c1} and s_{c2} are the slip values at the ultimate and residual bond strength, respectively. α is defined as a shape factor. Unlike the bond model proposed for unconfined concrete, two more variables were included in the confined bond-slip relation; those were f_e and β_c, indicating confinement pressure provided by transverse reinforcement and confinement factor, respectively. In this study, the effective lateral confining pressure was computed according to Mander *et al.* [33].

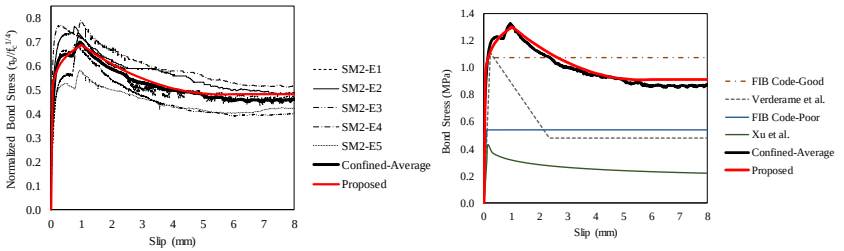

(a) (b)

Fig. 6.6. (a) Proposed bond-slip model for confined concrete under monotonic loading (b) comparison with available models

6.3 Bond-Slip Relation for Cyclic Loading

6.3.1 Proposed Bond Model for Unconfined Concrete

Similar to the methodology described in the previous section, the bond-slip relationship under cyclic loading was evaluated from experimental data. The bond stress was computed as the ratio between the axial force in the reinforcing bar and surface area (Fig. 6.7 and Fig. 6.8).

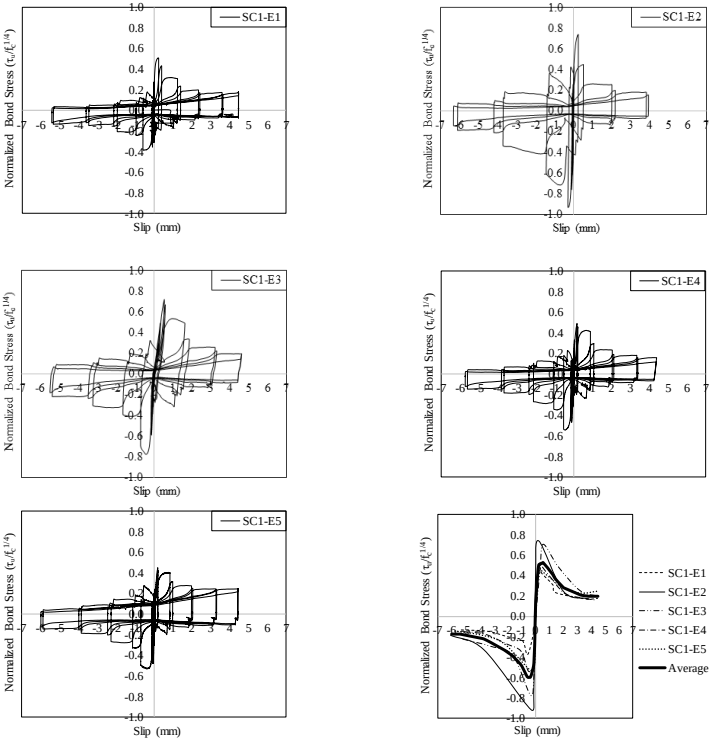

Fig. 6.7. Hysteric bond stress-slip response of unconfined specimens

The bond-slip relationship of the unconfined test specimens under cyclic loading was evaluated from the positive envelope curves, which is as follows:

$$\tau_u(s) = \begin{cases} \tau_{u1}\left(\dfrac{s}{s_{u1}}\right)^{\alpha} & if\ s < s_{u1} \\ 0.027s^2 - 0.23s + 0.65 & if\ s_{u1} \le s \le s_{u2} \\ \tau_{u2} & otherwise \end{cases} \quad \text{Eq. 6.12}$$

where the variables in the formula defined as follows:

$$\tau_{u1} = 0.56 f_c^{1/4} \quad \text{Eq. 6.13}$$

$$\tau_{u2} = 0.43 \times \tau_{uc1} \quad \text{Eq. 6.14}$$

$$\alpha = 0.42 \quad \text{Eq. 6.15}$$

$$s_{u1} = \sqrt{\frac{f_c}{80}} \quad s_{u2} = 2.5 \quad \text{Eq. 6.16}$$

Here, τ_{u1} and τ_{u2} are the maximum and residual bond strength values. s_{u1} and s_{u2} are the slip values at the ultimate and residual bond strength, respectively. α is a shape factor.

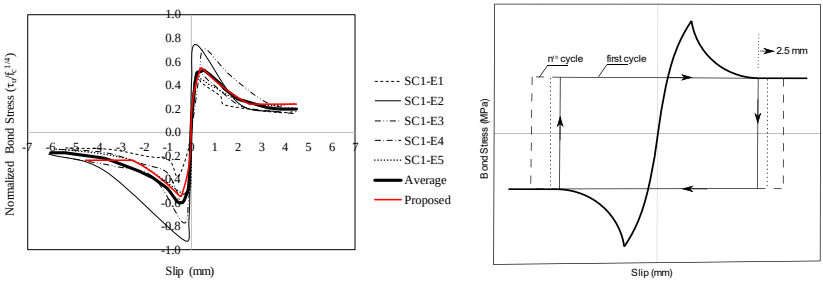

(a) (b)

Fig. 6.8. (a) Proposed bond-slip model for unconfined concrete under cyclic loading (b) schematic representation

6.3.2 Proposed Bond Model for Confined Concrete

The confined specimens under cyclic loading displayed a poor bond performance. The bond strength degraded suddenly and then it remained constant (i.e., residual part). When the load was exerted in the reverse direction, the slip value did not change considerably. On the other hand, the bond stress changed its sign. The semi-circle phenomenon was established under the cyclic action (Fig. 6.9). The proposed relationship was, yet again, obtained only for the positive loading direction. The hysteric bond-slip behavior was considered by the semi-circles' phenomenon in the proposed bond-slip relationship, which can be implemented by *Memory Bond Material* in ATENA [1]. It is assumed that the first critical-inversion slip occurred at 3.0 mm (Fig. 6.10). This value corresponds to the start of the residual bond stress value.

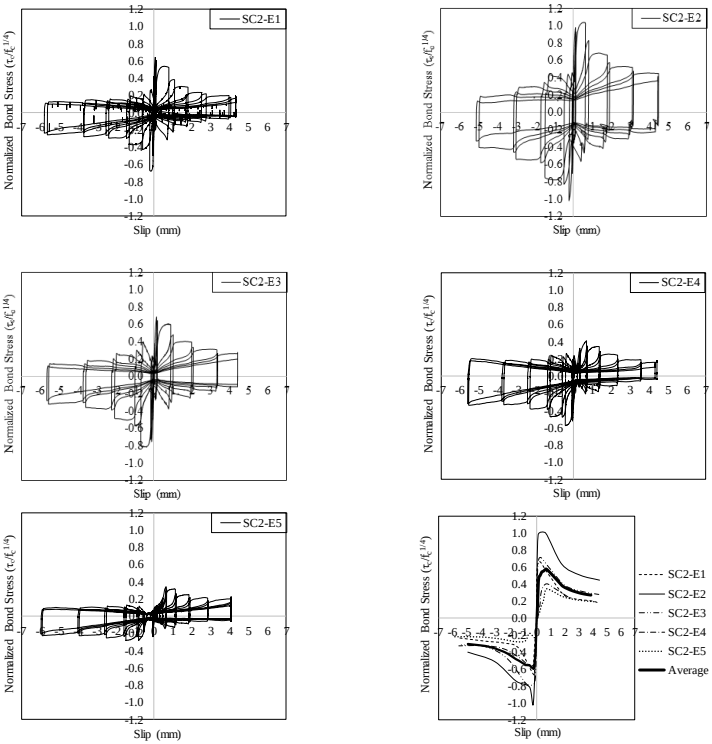

Fig. 6.9. Hysteric bond stress-slip response of confined specimens

The equation of a three-segment curve was provided in Eq. 6.17

$$\tau_c(s) = \begin{cases} \beta_c \times \tau_{c1}\left(\frac{s}{s_{c1}}\right)^{\alpha} & if\ s < s_{c1} \\ \beta_c \times [0.046s^2 - 0.29s + 0.77] & if\ s_{c1} \le s \le s_{c2} \\ \beta_c \times \tau_{c2} & otherwise \end{cases} \quad \text{Eq. 6.17}$$

where the variables in the formula defined as follows:

$$\tau_{c1} = 0.60 f_c^{\,1/4} \quad \text{Eq. 6.18}$$

$$\tau_{c2} = 0.5 \times \tau_{c1} \quad \text{Eq. 6.19}$$

$$\alpha = 0.22 \quad \text{Eq. 6.20}$$

$$s_{c1} = \sqrt{\frac{f_c}{30}}\ \ s_{c2} = 3.0 \quad \text{Eq. 6.21}$$

$$\beta_c = 0.855 e^{\left.f_e\right/ f_c^{\frac{2}{3}}}\ for\ f_e \ge 0.05 \quad \text{Eq. 6.22}$$

Here, τ_{c1} and τ_{c2} are the maximum and residual bond strength values. s_{c1} and s_{c2} are the slip values at the ultimate and residual bond strength, respectively. α is a shape factor. f_e and β_c indicating confinement pressure provided by transverse reinforcement and confinement factor, respectively.

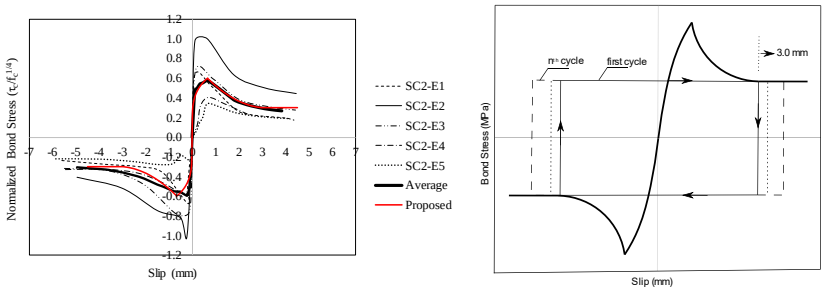

(a) (b)

Fig. 6.10. (a) Proposed bond-slip model for confined concrete under cyclic loading (b) schematic representation

6.4 Effect of Confinement on Bond-Slip Response

The complete loss of adhesion between the plain round bar and surrounding concrete occurred before reaching the tensile strength of the concrete f_{ct}. The microcracks took place in the contact area, which significantly violates the cohesion. Due to lateral confinement provided by the transverse reinforcement, which enhanced the concrete mechanical properties, the microcrack initiation was delayed or somehow minimized, which contributes cohesion in between the reinforcing steel and surrounding concrete. Therefore, a higher ultimate bond strength was computed for the confined concrete (Fig. 6.11a and b). The lateral confinement provided by the transverse reinforcement also changed the post-peak response. The nonlinear descending part of the bond-slip model for the confined concrete diminishes less steeply than the unconfined concrete. The slip corresponding to the bond stresses at transition zones differed as well. The residual bond strength formed at higher values for the confined case.

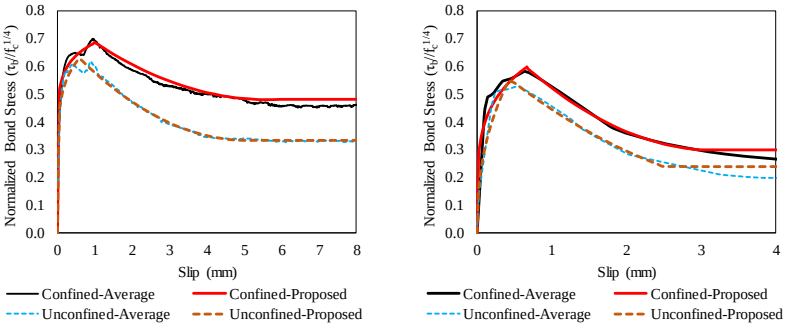

Fig. 6.11. Comparison of bond-slip models in confined and unconfined cases (a) monotonic loading (b) cyclic loading

6.5 Effect of Loading Scheme

The influence of the loading scheme on the response of the RC structures is essential as the deformation capacity of them differs under cyclic and monotonic loading. This partially violates the interaction between reinforcing steel and the surrounding concrete, which adversely affects the structural integrity. The monotonic and envelope of cyclic curves followed almost the same path in the initial loading stages while the gap widened remarkably at peak response. The significant bond degradation due to the nature of cyclic loading was more pronounced, especially in the post-peak region (Fig. 6.12a and b). The failure came out earlier under cyclic loading.

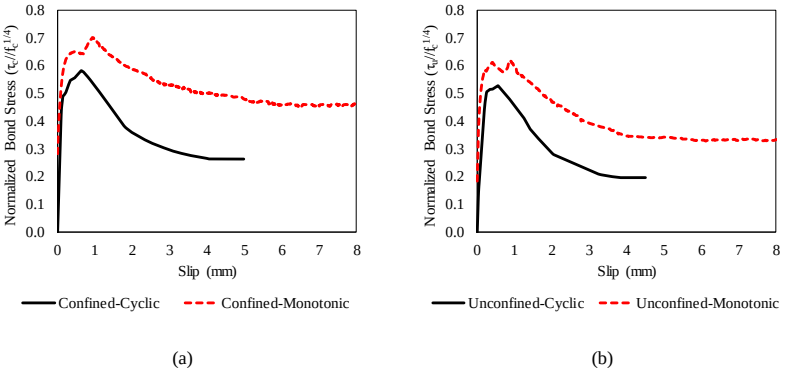

Fig. 6.12. Effect of loading scheme (a) unconfined concrete (b) confined concrete

6.6 Randomized Behavior under Monotonic Loading

The peak loads observed in the experiments were either at the edges of the bundle or within the upper and lower boundaries of the stochastic assessment (Fig. 6.13a and b). The post-peak response was accurately captured by the stochastic approach in the confined specimen, while the unconfined specimen SM1-E1 imparted a significant strength deterioration. It, therefore, fell out of the stochastic bundle. The remaining samples in the unconfined test series were simulated at an acceptable level.

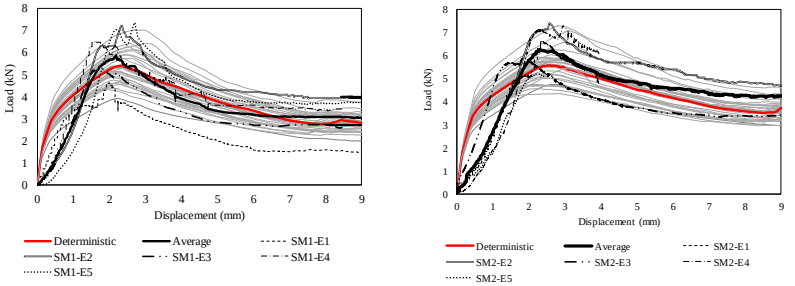

(a) (b)

Fig. 6.13. Randomized behavior under monotonic loading (a) unconfined case (b) confined case

The PDFs corresponding to the ultimate loads, together with the mean and standard deviation, were determined from the stochastic bundle, which were then compared with the experimentally obtained capacities (Fig. 6.14a and b). The dispersion in the capacity distribution was accurately characterized by the stochastic model.

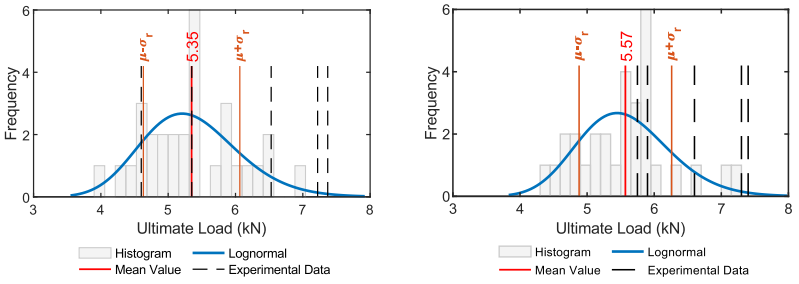

(a) (b)

Fig. 6.14. PDFs of ultimate load under monotonic loading (a) unconfined case (b) confined case

6.7 Randomized Behavior under Cyclic Loading

The ultimate capacity was satisfactorily captured by the FE solution; on the other hand, the displacement corresponding to the ultimate load was not accurately reproduced. The strength degradation was not characterized as well (Fig. 6.15a and b). The PDFs of the ultimate load were obtained from the ultimate capacity of each FE solution. Therefore, a good match in the peak response yields an accurate estimation of basic statistical characteristics.

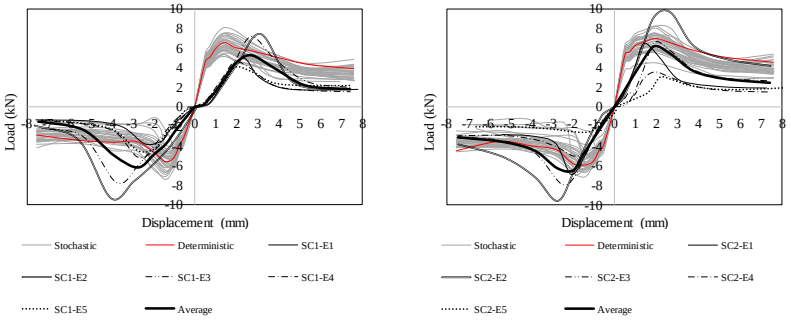

(a) (b)

Fig. 6.15. Randomized behavior under cyclic loading for (a) unconfined case (b) confined case

The PDFs of the ultimate strength were obtained from the stochastic bundle. Experimental capacities were then compared with the stochastic assessment (Fig. 6.16a and b). Note that if n likely specimens were tested n^{th} times under the same conditions, assuming that n is a relatively large number, similar statistical outcomes of the tests (mean, standard deviation, and PDFs) would be expected. Therefore, it is expected that the experimental results would be within the range of the PDF if the scatter was accurately reproduced by the stochastic assessment. On the other hand, some of the test results were not covered by the PDFs.

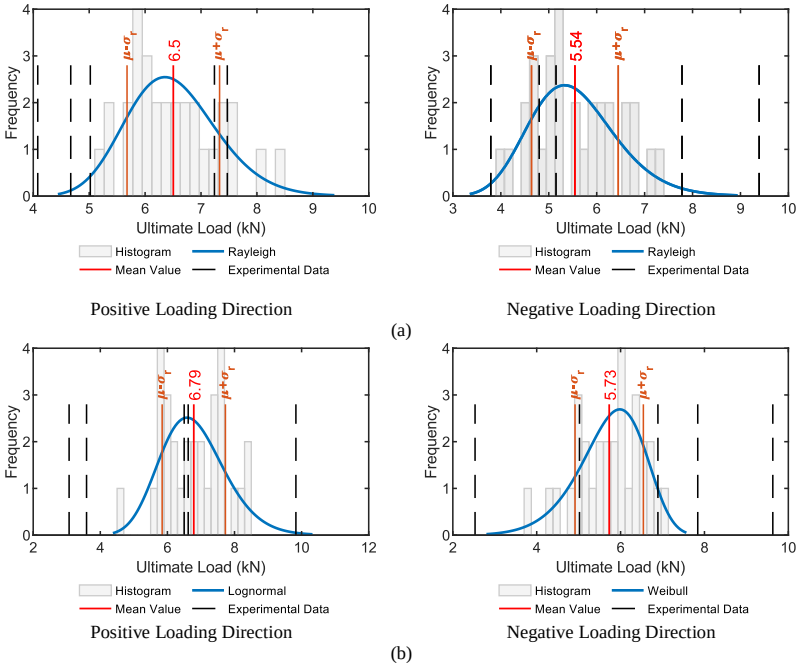

Fig. 6.16. PDFs of ultimate load under cyclic loading (a) unconfined case (b) confined case

6.8 Sensitivity Analysis

The highest correlation coefficient was computed for the concrete tensile strength f_{ct} in both monotonic and cyclic loading cases (Fig. 6.17a and b). The compressive strength of the concrete f_c contributes to the overall response with a medium impact. The remaining material parameters had little or no influence on the global response as the partial correlation coefficient was nearly zero.

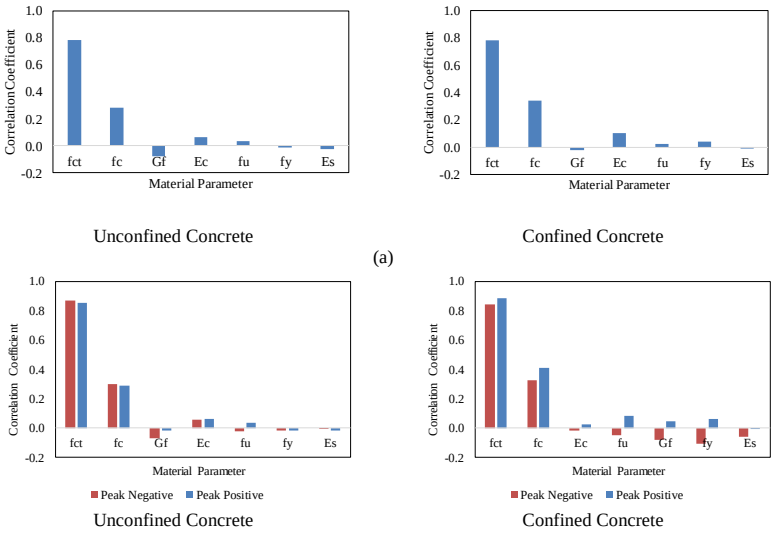

Fig. 6.17. Sensitivity analysis (a) monotonic loading (b) cyclic loading

7 CONCLUSION

This study mainly deals with the assessment of different failure modes in substandard RC members by stochastic approaches. The nonlinear FEM was combined with a suitable stochastic sampling technique for the realistic prediction of the structural response of substandard RC members. The effect of inherent uncertainties on the material mechanical properties was studied using an uncertainty analysis, which also leads to obtaining the basic statistics of response variables. The sensitivity of material properties on the global response was also measured by evaluating the partial correlation coefficient between material parameters (i.e., input variable) and the strength of the member (i.e., response variable). Moreover, the uneven distribution of concrete mechanical properties over the specimen was accurately characterized by random fields theory, which establishes weaker and stronger spots over the specimen.

This research context was organized into seven main chapters. The first three chapters dealt with the motivation for the research, numerical modeling strategy, and stochastic-based analysis methods. The following three chapters introduced the implementation of the advanced assessment strategy on different

substandard RC members. Each chapter was identical in terms of the method employed for stochastic assessment, while the test programs and resulting failure modes were different. Note that a section which summarizes the relevant chapter was included at the end of each chapter. The first testing program dealt with the performance of over-reinforced and shear critical beams. The experimental behavior was accurately reproduced in the FE environment. The effect of inherent uncertainties at a material level for over-reinforced and shear critical beam and uneven distribution of concrete mechanical properties over the shear critical beam were handled by a stochastic approach. This led to a more accurate assessment of the results. The shear critical and CFRP retrofitted beam-column joints were analyzed in the following chapter. The experimental performances were closely estimated by the numerical solutions. The relative impact of each material properties on the global response was also provided, which remarked the most critical material parameters. The last testing program focused on the stochastic-based numerical prediction of beam-type RILEM bond specimens. Thus, the proposed bond stress-slip relationship was implemented in the FE software and then evaluated to the stochastic level. The variability in the identical tests was characterized accurately by the stochastic assessment. The experimental results were covered by the stochastic bundle.

To conclude, owing to the more realistic assessment capability of the stochastic-based nonlinear FE analysis, which is now available in user-friendly computer tools, reproducing the structural response of substandard members by computational stochastic mechanics could yield more accurate results for assessment purposes. Overall, this study showed the efficiency of the advanced modeling strategy in different substandard RC members.

REFERENCES

[1] ATENA Program Documentation, Part 1. Atena theory manual, Cervenka Consulting, http://www.cervenka.cz/. 2014.

[2] Van Mier JGM. Multiaxial strain-softening of concrete, Part I: Fracture. Materials and Structures, RILEM 1986;19.

[3] Vecchio FJ, Collins MP. Modified compression-field theory for reinforced concrete beams subjected to shear. ACI Journal 1986;83:219–31.

[4] Kollegger J, Mehlhorn G. Experimentelle und analytische untersuchungen zur aufstellung eines materialmodels für gerissene stahbetonscheiben. Nr.6 Forschungsbericht, Massivbau, Gesamthochschule Kassel: 1988.

[5] Menetrey Ph, Willam KJ. Triaxial failure criterion for concrete and its generalization. ACI, Structural Journal 1995;92:311–8. doi:10.14359/1132.

[6] Hordijk DA. Local approach to fatigue of concrete. Ph.D. Thesis, Delft University of Technology, Netherlands: 1991.

[7] Bazant Z, Oh B. Crack band theory for fracture of concrete. Materials and Structures 1983;16:155–77.

[8] CEB-FIP Model Code. Comittee Euro-International du Beton, Bulletin d'information. 2010.

[9] Menegotto M, Pinto PE. Method of analysis for cyclically loaded reinforced concrete plane frames including changes in geometry and non-elastic behaviour of elements under combined normal force and bending. International Association of Bridge and Structural Engineering (IABSE), Lisbon, Portugal, vol. 13, 1973, p. 15–22.

[10] ATENA Program Documentation Part 4-9. ATENA Science – GiD Strengthening of concrete structures, Step by step guide for modelling strengthening with ATENA and GiD, http://www.cervenka.cz/. 2016.

[11] Mohr O. Welch umsttinde bedingen die elastizitltsgrenze und den bruch eines materials? Zeitschrift Des Vereins Deutscher Ingenieure 1900;44–45:1524-1530;1572-1577.

[12] Pukl R, Sajdlova T, Routil L, Novák D, Seda P. Case study – Nonlinear reliability analysis of a concrete bridge. Maintenance, Monitoring, Safety, Risk and Resilience of Bridges and Bridge Networks: Proceedings of the 8th International Conference on Bridge Maintenance, Safety and Management (IABMAS2016), 2016.

[13] fib Bulletin No.22. Monitoring and safety evaluation of existing concrete structures. 2003.

[14] Gulbrandsen P. Reliability analysis of the flexural capacity of fiber reinforced polymer bars in concrete beams, M.Sc. Thesis. University of Minnesota, 2005.
[15] Atadero RA, Karbhari VM. Sources of uncertainty and design values for field-manufactured FRP. Composite Structures 2009;89:83–93. doi:10.1016/j.compstruct.2008.07.001.
[16] Baji H, Ronagh HR, Li CQ. Probabilistic design models for ultimate strength and strain of FRP-confined concrete. Journal of Composites for Construction 2016;20:04016051. doi:10.1061/(ASCE)CC.1943-5614.0000704.
[17] Joint Committee on Structural Safety. Probabilistic model code, Part 3: Material properties. http://www.jcss.byg.dtu.dk; 2000.
[18] ACI 318M-11. Building code requirements for structural concrete and commentary (aci 318m-11), USA: American Concrete Institute. 2011.
[19] Duran B, Tunaboyu O, Avşar Ö. Determination of elasticity modulus of low strength concrete and its effect on the risk assessment results by DSVB. Journal of The Faculty of Engineering and Architecture of Gazi University 2017;32:253–64. doi:10.17341/gazimmfd.300617.
[20] Griffiths R, Holloway DG. The fracture energy of some epoxy resin materials. Journal of Materials Science 1970;5:302–307.
[21] Vořechovský M. Interplay of size effects in concrete specimens under tension studied via computational stochastic fracture mechanics. International Journal of Solids and Structures 2007;44:2715–31. doi:10.1016/j.ijsolstr.2006.08.019.
[22] Novák D, Vořechovský M, Rusina R. FReET v.1.5 – program documentation. User´s and Theory Guides. http://www.freet.cz. Brno/Červenka Consulting, Czech Republic: 2015.
[23] SARA Studio. SARA (Structural Analysis and Reliability Assessment) User's Manual. http://www.cervenka.cz/; 2015.
[24] EN 1992-1-1. Eurocode 2: Design of concrete structures - Part 1-1: General rules and rules for buildings. 2004.
[25] Yurdakul Ö. Experimental study on the investigation of strengthening the insufficient reinforced concrete beam-column joints by post-tensioning. M.Sc. Thesis. Civil Engineering Program, Graduate School of Sciences, Anadolu University, 2015.
[26] Yurdakul O, Avsar O. Structural repairing of damaged reinforced concrete beam-column assemblies with CFRPs. Structural Engineering and Mechanics 2015;54:521–43. doi:10.12989/sem.2015.54.3.521.
[27] Yurdakul Ö, Avşar Ö. Strengthening of substandard reinforced concrete beam-column joints by external post-tension rods. Engineering Structures 2016;107:9–22. doi:10.1016/j.engstruct.2015.11.004.

[28] Yurdakul Ö, Tunaboyu O, Avşar Ö. Retrofit of non-seismically designed beam-column joints by post-tensioned superelastic shape memory alloy bars. Bulletin of Earthquake Engineering 2018;16:5279–307. doi:10.1007/s10518-018-0323-y.
[29] El-Amoury T, Ghobarah A. Seismic rehabilitation of beam–column joint using GFRP sheets. Engineering Structures 2002;24:1397–1407.
[30] RILEM TC. RC 5 Bond test for reinforcement steel. 1. Beam test, 1982. RILEM recommendations for the testing and use of constructions materials, E & FN SPON; 1994.
[31] EN 10080. Steel for the reinforcement of concrete - Weldable reinforcing steel - General. 2005.
[32] Soleymani Ashtiani M, Dhakal RP, Scott AN, Bull DK. Cyclic beam bending test for assessment of bond–slip behaviour. Engineering Structures 2013;56:1684–97. doi:10.1016/j.engstruct.2013.08.005.
[33] Mander JB, Priestley MJN, Park R. Theoretical stress-strain model for confined concrete. Journal of Structural Engineering 1988;114:1804–26. doi:10.1061/(ASCE)0733-9445(1988)114:8(1804).